JOURNAL OF PROPULSION AND POWER
Vol. 25, No. 2, March–April 2009

Twin-Fluid Atomization and Novel Lifted Swirl-Stabilized Spray Flames

Martin B. Linck* and Ashwani K. Gupta†
University of Maryland, College Park, Maryland 20742

DOI: 10.2514/1.35723

The effects of swirl configuration and airflow distribution on the structure of swirl-stabilized spray flames are investigated in a combustor featuring a twin-fluid fuel atomization nozzle, coannular airstreams, and helical-vane swirl assemblies. The flames investigated are similar to those employed in gas turbine combustion engines. A novel lifted swirl-stabilized spray flame, obtained with a particular set of experimental conditions, is described. Three-dimensional particle image velocimetry data are used to analyze the structure of the airflow associated with the lifted flame. The lifting effect is shown to result from an interaction between the atomization airstream and the recirculation zone in the flow, which creates two distinct recirculation regions. Only the larger far-field recirculation zone is able to stabilize combustion effectively, and the structure of the airflow is found to determine the regions of heat release associated with the flame. Detailed information on the structure and characteristics of the fuel spray, obtained using phase-Doppler particle analysis, is also presented. The twin-fluid atomization approach is shown to provide effective atomization over a wide range of operating conditions, while simultaneously allowing a great degree of control over the flame structure.

Nomenclature

$D10$	=	arithmetic mean diameter
$D32$	=	Sauter mean diameter
G_Z	=	axial momentum of flow
G_θ	=	angular momentum of flow
h	=	swirler height
L	=	characteristic length scale
p	=	local pressure
p_∞	=	ambient pressure
Re	=	Reynolds number
R_c	=	swirler central radius
R_i	=	inner radius
R_o	=	outer radius
r	=	radial location
S	=	swirl number
t_Z	=	translation of a helical assembly in units of length
U	=	mean radial velocity
V	=	mean axial velocity
v'	=	fluctuating component of axial velocity
W	=	mean tangential velocity
w'	=	fluctuating component of tangential velocity
δ	=	air annulus width
δ_i	=	inner air annulus width
δ_o	=	outer air annulus width
θ_r	=	rotation of a helical assembly in degrees
θ_B	=	swirler local blade angle
θ_o	=	swirler outer blade angle
μ	=	dynamic viscosity
ρ	=	local density

Received 16 November 2007; revision received 21 September 2008; accepted for publication 10 October 2008.

*Graduate Researcher, Department of Mechanical Engineering. Student Member AIAA.

†Distinguished University Professor, Department of Mechanical Engineering. Fellow AIAA.

I. Introduction

SWIRL-STABILIZED flames have been found to possess extremely useful characteristics, such as large turndown ratios, rapid fuel vaporization, and efficient mixing, thus allowing the design of compact and stable combustion systems [1]. The investigation described here deals with the behavior of a swirl-stabilized, methanol-fueled combustor, which features a swirl-stabilization arrangement found in many compact high-energy-density combustors, such as those in gas turbine engines.

Essential observations on the nature and characteristics of swirling flows have been presented by Gupta et al. [1]. In a swirling flow, the rotation of the fluid plays a significant role in determining the structure and behavior of the flow. The centrifugal force created by the rotation of the fluid forces the flow toward the outer walls of the duct. The degree of rotation of a flow can be characterized by the swirl number S, which is a nondimensionalized ratio between the mean axial momentum and mean angular momentum of the flow [1]:

$$S = \frac{G_\theta}{G_z \times L} \tag{1}$$

where G_θ is the angular momentum, G_Z is the axial momentum, and L is a characteristic length associated with the flow (usually the duct diameter). In a situation in which the flow is annular, the inner and outer radii of the annulus are referred to as R_i and R_o, respectively. An approach by which the swirl number of a flow can be obtained is presented next [1]:

$$S = \frac{G_\theta}{G_z \times R_o} \tag{2}$$

$$G_\theta = \int_{R_i}^{R_o} (\rho \times V \times W + \rho \times \overline{v' \times w'}) \times r^2 \mathrm{d}r \tag{3}$$

$$G_z = \int_{R_i}^{R_o} (\rho \times V^2 + \rho \times \overline{v'^2} + (p - p_\infty)) \mathrm{d}r \tag{4}$$

In this approach, V and W represent the axial and angular components of the mean velocity. The fluctuating components of velocity in the axial and angular directions are represented by v' and w'. The local density is denoted by ρ, the local pressure is represented by p, the pressure of the ambient surrounding the flow is denoted by

p_∞, and the variable r indicates radial location. However, this expression contains several terms in Eqs. (3) and (4) that cannot generally be obtained experimentally. The local density ρ is not usually available and, in practice, is generally assumed to be a constant. The pressure is assumed to be a constant as well. The turbulent shear stress term, which depends on the correlation between v' and w' in Eq. (3), is also difficult to measure experimentally. Thus, the pressure-dependent term and the term involving the shear stress are generally omitted in the calculation of the swirl number, and an approximate swirl number can be obtained on the basis of mean axial and radial velocities as a function of radial location, as shown in Eq. (5):

$$S = \frac{\int_{R_i}^{R_o} V \times W \times r^2 \mathrm{d}r}{R_o \times \int_{R_i}^{R_o} V^2 \mathrm{d}r} \tag{5}$$

This approximate swirl number is accurate to within 2–3% of the value obtained when the full expressions, including the turbulence-related terms, are used [2]. Flows are generally compared in the literature on the basis of swirl numbers calculated at the exit plane of the duct from which the rotating flow emerges.

Flows with high swirl numbers are found to display characteristics that have proven to be very useful in the field of combustion. If the swirl number of a simple flow emerging from a round duct is greater than 0.6, the flow displays vortex breakdown [3]. In this situation, the pressure at the center of the flow is reduced dramatically by the rotation. Fluid from the downstream region, which has a lower velocity and therefore a higher pressure, is forced back upstream, forming a recirculation region in the flow. In a combustor, this recirculating material helps to ignite the relatively cold incoming material, and this makes it possible to stabilize a flame in the combustor at much higher fuel and airflow rates than would otherwise be possible. In cases in which there is a central obstruction in the flow, such as a fuel nozzle or bluff-body flame stabilizer, some recirculation downstream of the obstruction would usually occur, even if the swirl number were zero. When rotation is imparted to the flow, this recirculation region downstream of the obstruction increases in size and combustion is stabilized more effectively [4]. The recirculation region in this case has a distinct tulip shape, and flames stabilized through this approach usually have the same shape.

The recirculating flow in the combustor is also quite turbulent, and this provides a useful degree of mixing. In nonpremixed combustors, in which the fuel and oxidizer are injected separately, rapid and complete mixing is desirable for high combustion efficiency to be achieved. A very effective strategy in combustion has been to inject gaseous or liquid fuel directly into the recirculation zone. If the fuel is injected as a liquid, the fuel droplets evaporate rapidly in the hot recirculating gas. This approach is often employed in gas turbine applications [5]. However, because the recirculated material consists largely of product gases, the concentration of unreacted oxidizer in the recirculation region is low. Ignition of the fuel does not occur until the heated vaporized fuel is brought into contact with unburned oxidizer at the boundary of the recirculation region. Turbulent distortions of the flow then mix the combusting material to promote rapid and complete combustion.

In previous studies of swirl-stabilized systems featuring a central obstruction, the flames have been attached to the object in the center of the flow. The region of the reaction zone closest to the obstruction interacts with it and may be quenched by its close proximity to the object. Such a flame is shown schematically in Fig. 1. This phenomenon may create considerable difficulties, because quenching of combustion reactions in this way may cause increases in unwanted emissions, excessive local heating of the combustor components, and sooting [6,7].

The problems associated with attached flames can be avoided if the flame is lifted. In a lifted flame, combustion does not occur near the central object. Instead, the flame is located some distance downstream of the object. Lifted swirl-stabilized flames, obtained in flows with a central obstruction, have not been described in the literature. The present investigation will demonstrate that a lifted flame can be obtained if a twin-fluid atomizing nozzle is used to inject a liquid fuel spray into a swirling flow with particular properties. This novel approach allows the control of swirling flow structure and flame in an entirely new way and may make it possible to create flames with more desirable characteristics.

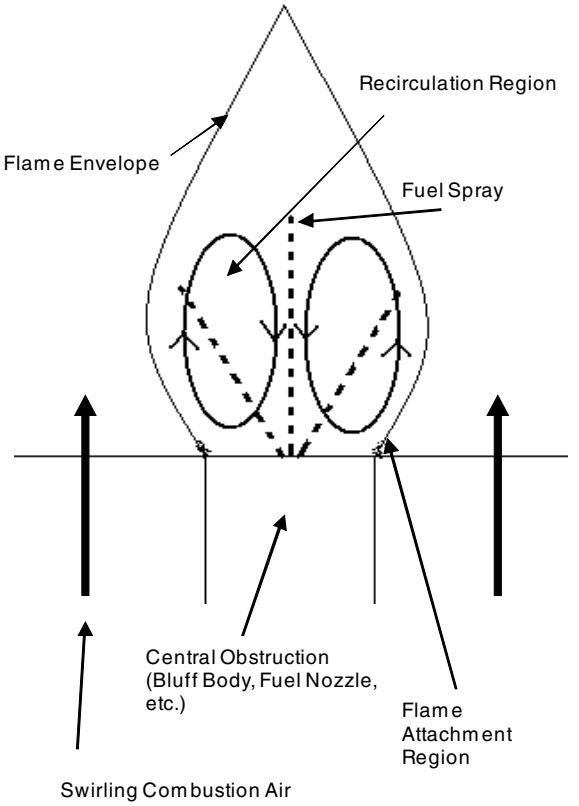

Fig. 1 Schematic of attached swirl-stabilized spray flame

II. Experimental Equipment

The combustor used to carry out the present investigations is shown schematically in Fig. 2. An injector assembly containing inner and outer air annuli and a centrally positioned twin-fluid atomizing nozzle was used to feed fuel and air into the system. The outer diameter D of the larger air annulus in the injector was 62 mm. Swirlers were installed at the exits of the air annuli through which the combustion air was fed. Atomization-air and fuel streams were injected into the combustor through the atomizing nozzle. The combustor was unenclosed in the investigation described here.

A commercially available fuel nozzle (type 30610-1, Delavan Spray Technologies) was used in this study. It was rated by the manufacturer to atomize 1.9 liter/h of water (or 0.5 gal/h), using an air pressure drop of 0.68 bar and an atomization-airflow rate of 22.6 standard liter/m. The nozzle produced a solid-cone spray, with a

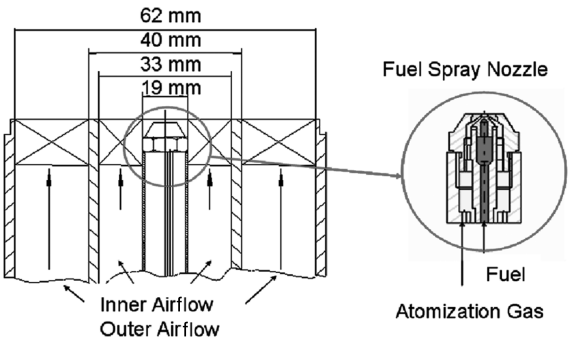

Fig. 2 Swirl-stabilized spray burner schematic, showing swirler assemblies and twin-fluid fuel nozzle.

mean droplet diameter of approximately 30 to 50 μm. In a twin-fluid atomizing nozzle of this type, the fuel stream is brought into contact with a rotating stream of atomizing air, for which the flow rate can be adjusted independently [8]. The atomization-airflow rate will generally represent less than 1% of the total air fed to the burner, but it is the only important parameter in determining the atomization characteristics of the nozzle.

To ensure that optical diagnostics could be applied in studies of the combustor, the entire system had to move in three dimensions, relative to the fixed optics. The combustor system was built on a three-dimensional positioning stage. The stage consisted of a heavy aluminum plate, 2.5 cm thick, which could be raised or lowered by means of four screw jacks positioned at the corners. The screw jacks were operated by a linked transmission so that all four jacks turned at the same time and at the same speed. The transmission was controlled by a high-precision stepper motor, and the y position (vertical height) of the combustor could thus be controlled with precision on the order of 1 μm. The total travel in the vertical direction was approximately 60 cm. A schematic of the experimental facility is shown in Fig. 3.

Translation in two horizontal directions, referred to as the x and z axes, was accomplished by building the combustor on a smaller platform on top of two linear positioning tracks, also controlled by stepper motors. These motors were geared differently from the one controlling the y position (or vertical elevation) of the burner and were used to position the system with a precision on the order of 2.5 μm.

The axes of motion of the burner were aligned with the axes of the optical diagnostic systems used in the experiments. The precision of the alignment was such that the burner could be translated 30 cm along the path of one of the lasers, with a lateral displacement away from the laser path of less than 100 μm. All three stepper motors were actuated by a single programmable controller unit.

Compressed air was supplied to the burner by a screw-drive compressor system. The air was regulated in two stages to control variation in the airflow rates to within less than 1% of their total value. The air handling system used to supply air to the burner is also shown in Fig. 3. Air from the compressor was fed at 85 psig to a set of choked-orifice flow-measurement devices. This approach was employed so that the inner combustion air, outer combustion air, and atomization airstreams were controlled and measured separately before being fed to the burner. Orifices made by O'Keefe Controls were installed in each line to produce the necessary choking conditions. The manufacturer-supplied orifice calibration was used to determine the flow rates. The pressure upstream of each orifice was measured using digital pressure gauges. The temperature of the air entering from the compressor was measured using a thermistor-type thermometer installed in the air line near the orifices.

Further steps were taken to introduce seeding material into the inner and outer combustion airstreams. For nonintrusive optical particle image velocimetry (PIV) studies of the motion of the nonreacting airflow associated with the combustor during operation, it was necessary to introduce marker particles into the flow so that the flow could be tracked. The seeding process and the properties of the droplets are discussed subsequently.

The methanol fuel supplied to the burner was stored in a pressurizable stainless-steel vessel. Fuel was then passed through a turbine flowmeter (MacMillan model G112). The fuel calibration was checked by direct flow rate measurements. A needle valve downstream of the flowmeter was used to control the flow rate. The flow rate of methanol was controlled to within 0.1 ml/ min.

The swirlers used to impart rotation to the airflows were of particular importance. To obtain a symmetrical flow, swirlers must be machined to very tight tolerances [9]. Swirl vanes may be flat or they may be curved in a variety of ways [1]. For this investigation, helical-vane swirlers were employed, as these are compact, can be inserted directly into an air duct, and can be machined from a single piece of stock without any further assembly steps. The degree of twist associated with helical-vane swirlers can be characterized by some amount of rotation θ_r in degrees per some lateral translation t_Z in units of length.

Each helical swirler had 12 vanes, and the vane thickness of each blade was approximately 1 mm. The vane thickness varied by a few microns from swirler to swirler, due to the different swirler geometries, but within each assembly, all vanes were of exactly the same thickness. The most important characteristic of any swirler is the outer blade angle, for the simple reason that centrifugal effects force rotating flows outward, and the swirl properties imparted to most of the air will depend on the properties of the swirl vanes near the outer wall of the duct [4]. In a flat-vane swirl assembly, the local blade angle, defined as the angle between the blade surface and the centerline of the swirler, is constant and does not vary with radial location. In a helical-vane assembly, the local blade angle varies with radial location r, due to the blade geometry. An expression for the local blade angle θ_B in a helical-vane assembly is given next:

$$\theta_B(r) = \tan^{-1}\left(\frac{\theta_r \times r}{t_Z}\right) \tag{6}$$

The outer blade angle θ_o of a helical swirl assembly can be found if the dimensions and the twist of the vanes are known:

$$\theta_o(r) = \theta_B(R_o) = \tan^{-1}\left(\frac{\theta_r \times R_o}{t_Z}\right) \tag{7}$$

The important dimensions of a helical-vane swirler are illustrated in Fig. 4. They are the central radius R_c, the inner radius R_i, the outer radius R_o, and the height h.

In the present work, the swirl number of each swirler was calculated on the basis of three-dimensional particle image velocimetry observations of flows emerging from each swirler assembly. These data are presented in the Results and Discussion section.

For purposes of comparison, each swirler was classified according to its outer vane angle and according to type (the two types being inner and outer). For example, a swirler designed to be inserted in the inner air duct and that features an outer vane angle of 45 deg is referred to as swirler 45-i. A swirler designed to be inserted into the

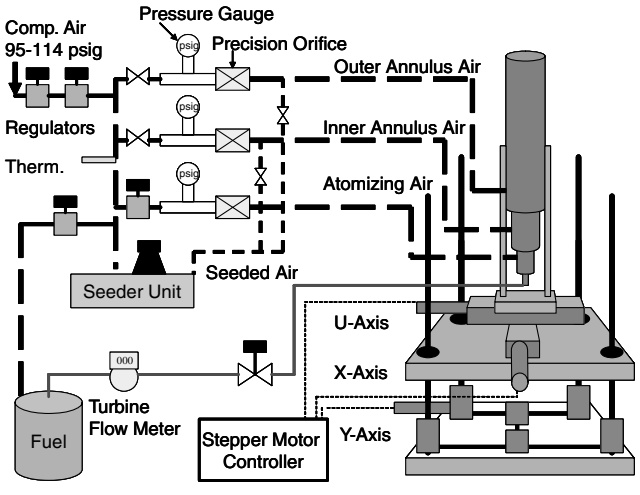

Fig. 3 Schematic of the experimental facility.

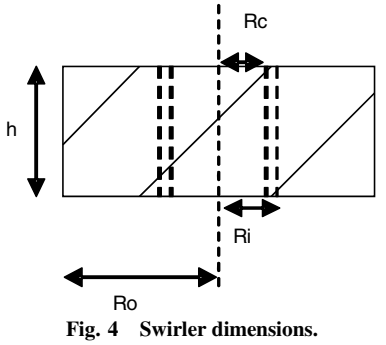

Fig. 4 Swirler dimensions.

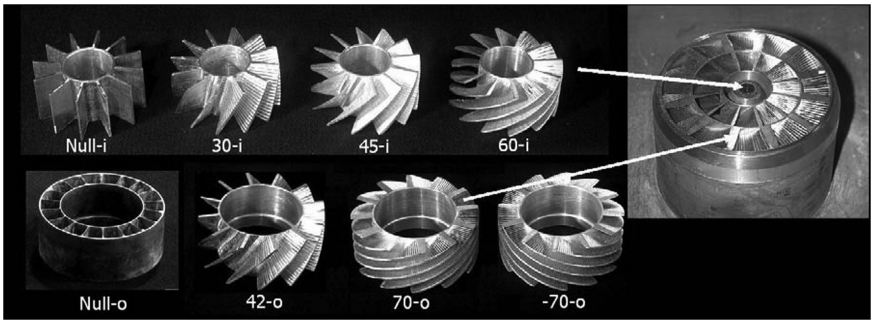

Fig. 5 Swirlers used in the swirl-stabilized spray burner.

outer air annulus and that features an outer vane angle of 42 deg is referred to as swirler 42-o.

Four inner and four outer swirlers were used in the course of the experiments described subsequently; they are shown in Fig. 5. The inner swirlers featured outer vane angles of 0, 30, 45 and 60 deg (from the vertical axis). The outer swirlers featured swirl angles of 0, 42, 70, and −70 deg (counterswirl).

Swirlers with a positive outer vane angle imparted counterclockwise rotation to the air (seen from the top into the burner), whereas the outer swirler with a negative vane angle (−70 deg) caused the air to rotate in a clockwise direction. This unique swirler was created so that the effect of counter-rotation on the structure of the flame could be examined. In a counter-rotating arrangement, the airstreams in the inner and outer annuli rotate in opposite directions. Swirler assemblies with a 0 deg swirl angle are essentially flow straighteners and are referred to here as null swirlers. The null-o swirler, shown in the second row in Fig. 5, shares the same dimensions as the other swirler assemblies. The dimensions and properties of the swirlers used in the current investigation are given in Table 1.

III. Diagnostics

A. Direct Flame Imaging

The global features of flames associated with the combustor were examined and recorded with a digital camera with a 3.3 megapixel detector. Aperture, exposure times, and focal length could all be controlled manually or automatically. Manual control was employed to optimize the images obtained. In the experiments described subsequently, a 0.5 s exposure time was used to record the flame images. The long exposure time was necessary for two reasons. First, methanol produces a flame with low luminosity. Second, the flames were quite turbulent, and it was found that a 0.5 s integration interval helped produce repeatable flame features from one image to the next. Flame luminosity is an indicator of heat release, and because the methanol flame produced sufficient observable radiation in the visible spectrum, the images obtained show the averaged regions of heat release associated with the flame. The images were scaled with the aid of reference exposures, wherein grids of known dimensions were photographed. These grids could then be overlaid onto the flame images. The main limitation was the number of pixels in the images. All dimensions associated with the flame images were accurate to within less than 1 mm.

B. Particle Image Velocimetry

PIV involves photographing light scattered by small seed particles present in a flow. The seed particles or droplets are illuminated by a laser sheet [10]. Three-dimensional (3-D) PIV depends on analysis of images from two cameras, so that the full three-dimensional data associated with the flow can be obtained. Each digital camera captures image pairs, and an algorithm produces a two-dimensional (2-D) vector field. Then each set of 2-D vector fields is analyzed to reconstruct the full 3-D vector field. A PIV system built by Integrated Design Technologies was used in these investigations.

To examine the behavior of the flows, the combustion airflows were seeded with polydisperse propylene glycol droplets with mean diameters in the 4–5 μm range. The droplets were produced using a TSI model 9306 six-jet atomizer [11]. The droplets were able to resolve turbulent structures occurring in the flow at scales that were approximately 30 times larger than the Kolmogorov scale and were thus able to provide useful information on mean velocities in the flow [12,13].[‡]

The flow was illuminated by a laser sheet obtained using a twin-cavity 532 nm pulse laser system, producing pulse energies from 50 to 200 mJ. The duration of each pulse was approximately 3–5 ns. The laser head was pumped and fired at 5 Hz, and the time interval between pulses was adjusted depending on the features of the flow.

The monochrome cameras used had a resolution of 1360 × 1036 pixels (1.4 megapixels). The pixel size on each detector was 4.7 μm. Each camera was fitted with a 532 nm narrow-band-pass filter and a mechanical shutter to ensure that only laser light reached the detector and to prevent overexposure of the second image in each image pair. The cameras were positioned on either side of the laser sheet to capture light at a 30 deg forward-scattering angle. This arrangement allowed each camera to image an examination region that extended 30 mm horizontally and 25 mm vertically above the burner. Two hundred image sets were obtained for each experiment, to obtain accurate measurements of mean velocity. Further details of the technique are provided by Linck [2].

Table 1 Properties of swirlers

Swirler	Type	R_i, mm	R_o	R_c, mm	h, mm	Twist, deg/mm	θ_o, deg
Null-i	Inner	9.53	19.82	8.71	18.71	0.00	0.0
30-I	Inner	9.53	19.82	8.71	18.71	1.69	30.3
45-I	Inner	9.53	19.82	8.71	18.71	2.83	44.5
60-I	Inner	9.53	19.82	8.71	18.71	5.06	60.3
Null-o	Outer	20.70	30.99	19.86	25.40	0.00	0.0
42-o	Outer	20.70	30.99	19.86	25.40	1.69	42.4
70-o	Outer	20.70	30.99	19.86	25.40	5.06	70.0
−70-o	Outer	20.70	30.99	19.86	25.40	−5.06	70.0

[‡]Private communication with J. Wallace, 2005.

C. Phase-Doppler Particle Analyzer

The fuel spray produced by the twin-fluid atomizing nozzle was investigated using a 2-D phase-Doppler particle analyzer (PDPA) manufactured by Aerometrics, Inc. [14]. The system provided two components of droplet motion, as well as droplet size information about each droplet measured. Details of this technique are given elsewhere [15]. The technique measured the size, as well as the velocity in the axial and radial directions, of individual droplets at particular locations in the spray.

A 300 mW argon-ion laser was used to create the necessary laser-measurement junction. Reliable information was obtained by allowing the instrument to acquire data for up to 2 min, or until 10,000 droplets had been measured at a given measurement location [16].

In the polydisperse sprays investigated here, the laser power and photomultiplier (PMT) voltage had to be optimized so that each channel was flooded less than 1% of the time at the point in the spray at which flooding of the channel was most likely to occur. Data were then acquired throughout the spray using these settings.

Each channel had to be calibrated at the correct PMT voltage setting using a calibration diode. Measured values were found to be very repeatable, particularly in regions in which the frequency of droplet acquisition was greater than 50 Hz. Mean diameters were found to vary by approximately 0.5 μm from one run to the next, and mean velocities varied by less than 1% between successive runs at any measurement location.

IV. Airflow Conditions

In this investigation, two airflow conditions were examined. The Reynolds number of the flow through each swirler depended on the volumetric flow rate of the air moving through the air annulus. For the first airflow condition (called airflow condition 1), 5.47 g/s of air were fed through each swirler. For the second airflow condition (called airflow condition 2), 9.3 g/s of air were fed through each swirler. The Reynolds number Re at the swirler inlet was calculated based on the width of the annulus δ, axial velocity, density, and dynamic viscosity of the flow μ:

$$Re = \frac{V \times \rho \times \delta}{\mu} \tag{8}$$

In the combustor, δ_i and d_o were the widths of the inner and outer annuli, respectively. The swirler inlet Reynolds numbers in airflow condition 1 were 3.23×10^3 and 1.8×10^3 in the inner and outer swirlers, respectively. The Reynolds number of the outer swirler was smaller, because the cross-sectional area of the outer swirler was larger than that of the inner swirler.

Airflow condition 2 featured 9.3 g/s of air passing through each swirler. The Reynolds numbers of the flows through the inner and outer annuli were 5.5×10^3 and 3.1×10^3, respectively. The relevant parameters of these experimental conditions are given in Table 2.

V. Results and Discussion

A. Swirl Numbers

To compare the results from this study with those of others in the literature, it was necessary to measure the swirl condition associated with the flow from each individual swirler. The swirl number was calculated using Eq. (5). All three components of velocity were obtained experimentally, and the axial and tangential mean velocities were integrated across the flow.

Table 2 Airflow conditions

	Airflow condition 1	Airflow condition 2
Inner-annulus mass flow rate	5.47 g/s	9.3 g/s
Outer-annulus mass flow rate	5.47 g/s	9.3 g/s
Inner-annulus volume flow rate	4.5 liter/s	7.7 liter/s
Outer-annulus volume flow rate	4.5 liter/s	7.7 liter/s
Inner-annulus average velocity	4.8 m/s	8.1 m/s
Outer-annulus average velocity	2.7 m/s	4.6 m/s
Inner-annulus Reynolds number	3.23×10^3	5.5×10^3
Outer-annulus Reynolds number	1.8×10^3	3.1×10^3

Contours of the mean axial, radial, and tangential velocities of the flow emerging from the 45-i swirler under both airflow conditions and with no flow emerging from the outer swirler are shown in Fig. 6. The structure of the airflow changed very little when the flow rate was changed. The values of the mean velocities scaled well with flow rate, but the shape of the flow contours did not change greatly. Interestingly, the contours of the flow were quite complex, due to the nature of the swirler. Because the flow emerged directly from the swirler, it was seen to form a series of adjacent spiraling jets, rather than a single smooth rotating column of air. The adjacent jets emerging from each open space between swirl vanes interacted and mixed as they proceeded downstream. Flows of this type have not been examined in detail in the literature, although they are representative of flows occurring in gas turbine combustors, in which the flow often emerges directly from the swirler unit and then interacts with the fuel spray.

The swirl numbers obtained by radially integrating mean air velocity values at an elevation 1 mm above each swirler, with the laser plane bisecting an open space between the vanes of each swirler, were also found to change only slightly when the airflow condition was changed. The changes observed were due to changes in boundary-layer thickness inside each swirler [2]. The swirl numbers of flows emerging from different swirlers at each airflow condition are given in Table 3.

B. Effect of Swirl Configuration on Flame Structure

The swirl configuration in the injector had a significant effect on flame structure, and to investigate this effect, 12 swirl configurations were examined at a single atomization airflow rate, airflow condition, and fuel flow rate. The flames associated with each swirl condition were photographed using an exposure time duration of 0.5 s.

The airflows were set so that airflow condition 2 was achieved. No seeding was present during this set of experiments. The fuel nozzle was supplied with 0.14 g/s of atomizing air to provide effective atomization of 31 ml/min of methanol. Assuming complete combustion, the thermal load of the flame was 8.2 kW.

Swirl conditions were categorized according to the inner and outer swirlers employed. The flames are shown in Fig. 7. They are grouped according to the outer swirler employed in each configuration. All four outer swirlers were employed. However, only the 30-i, 45-i, and 60-i swirlers were used here. It was found that if the null-i swirler was used, no stable flame could be obtained with the combustion airflow rates used here. Even in the case of the 30-i swirler, a flame was stabilized only if used in combination with the 70-o or −70-o (counter) swirlers. These combustion airflow rates were selected to approximate overall fuel-lean equivalence ratios. If these flows had been introduced into a sealed combustor (as opposed to the unenclosed conditions described here), the equivalence ratio would have been 0.35.

All the flames obtained were between 150 and 240 mm in length. The maximum width of each of the flames was comparable, with each flame displaying a maximum diameter of approximately 40–60 mm.

In the cases in which a small outer swirl angle was employed (null-o or 42-o), the flame geometry depended primarily on the geometry of the inner swirler. In cases in which the outer swirl angle was large (70-o or −70-o), the flames obtained with each inner swirler did not vary dramatically in size or shape. The counterswirling flames obtained with the −70-o outer swirler did not vary dramatically from their coswirling counterparts, though the flame region did appear to be slightly shorter. This may indicate that mixing of fuel and oxidizer occurs more rapidly in the counterswirling flames.

The most compact flame obtained was achieved by use of the 45-i/null-o configuration, with the visible flame terminating 150 mm downstream of the fuel nozzle exit. This flame was also lifted, with combustion beginning 30 mm downstream of the fuel nozzle. This

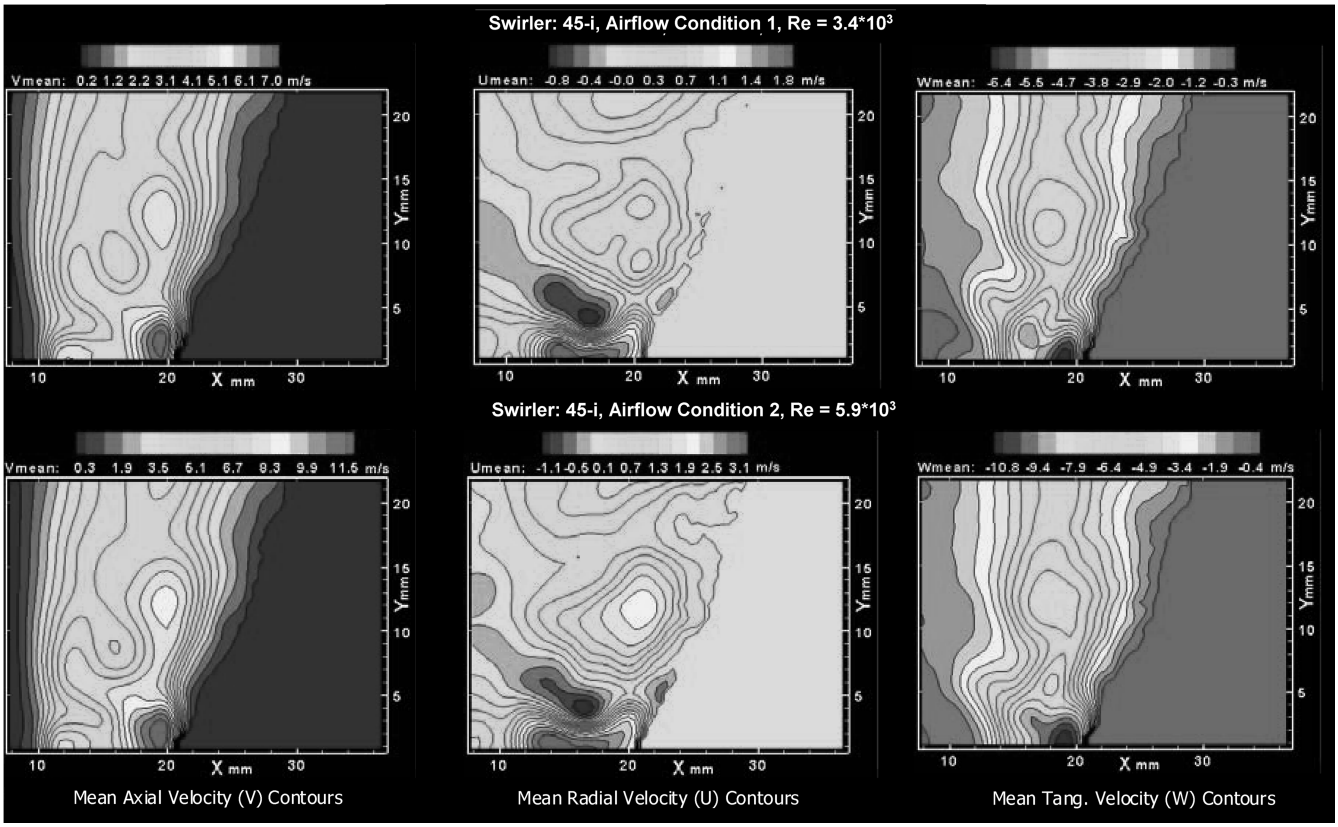

Fig. 6 Mean axial, radial, and tangential, velocity contours of flows emerging from 45-i swirler at two different airflow conditions.

lifting effect was extremely interesting, because lifted swirl-stabilized flames formed downstream of an obstruction in the flow have not been observed before [1,3–5]. The presence of the atomizing air from the fuel nozzle was an additional factor in this case. The effect of the atomizing-air jet on the flow, in both the nonreacting and reacting cases, was investigated further to examine this lifting effect.

C. Structure of a Lifted Flame and the Effect of the Atomizing-Air Jet on the Recirculation Zone

The 3-D PIV technique was used to understand the structure of the 45-i/null-o flowfield. The PIV technique cannot be applied effectively if a fuel spray is present. The fuel droplets are generally much larger than the seeding droplets and do not faithfully follow the airflow. The PIV images obtained in such a case could provide information on the features of the fuel spray [17], but would not allow the real flowfield of the gaseous phase to be examined. A fuel spray is inherently necessary for combustion to occur, however, and so only the nonreacting-airflow field could be conveniently observed. Because the structure of the flame is closely linked to the features of the airflow field, the nonreacting airflow provides important information in the analysis of the flame structure, as shown subsequently.

A series of observations were carried out using the 45-i/null-o swirl configuration. A region of the flow extending from the centerline to a maximum radial distance of 30 mm was examined.

Table 3 Swirl number *S*

Swirler	Airflow condition 1	Airflow condition 2
30-i	0.4	0.4
45-i	0.7	0.8
60-i	1.1	1.2
42-o	0.5	0.6
70-o	1.6	1.7

Axial locations from 1 to 24 mm downstream from the swirler exit plane were examined. Both airflow conditions and three atomization-airflow-rate cases were examined. The atomization-airflow rate in each case was scaled according to the airflow condition, to examine whether similar flow structures could be created across a range of flow conditions when a central atomization-air jet was present.

In the first atomization-air case (called atom.-air case 1), the flow rate of atomization air was 0 g/s for both airflow conditions. In the second case (called atom.-air case 2), the flow rate of atomization air was 0.04 g/s for airflow condition 1 and 0.08 g/s for airflow condition 2. Atom.-air case 3 provided 0.07 g/s of air for airflow condition 1 and 0.14 g/s of air for airflow condition 2. The relationship between the airflow conditions and atomization-air cases is given in Table 4.

The objective of this approach was to examine scaling. If the effect of the atomization jet on the flowfield can be scaled with Reynolds number, then the flowfield geometry can be controlled by controlling the atomization-airflow rate, and a uniform flowfield can be established across a range of flow rates.

Figure 8 shows a comparison of axial velocity contours at both airflow conditions using atom.-air cases 1 and 2. In atom.-air case 1, the recirculation region in both flows extended all the way down to the atomization nozzle. In atom.-air case 2, a scaled atomization airflow was present. This flow emerged from the fuel nozzle at the centerline and produced the positive axial velocities seen at the centerline and extending 10 mm upward into the flow. For both airflow conditions, the presence of atomization air produced the same effect on the recirculation region. Two separate recirculation regions were produced: one confined to the region immediately surrounding the fuel nozzle and the other extended further downstream. These are referred to as the near-field and far-field recirculation regions, respectively.

Given that the effect of the atomization-air jet can be scaled with the flow rate of the swirling flow, all three atomization cases were examined at a single airflow condition. Figure 9 shows comparisons of mean axial velocity contours associated with the three atomization-air cases under airflow condition 2. Atom.-air case 3

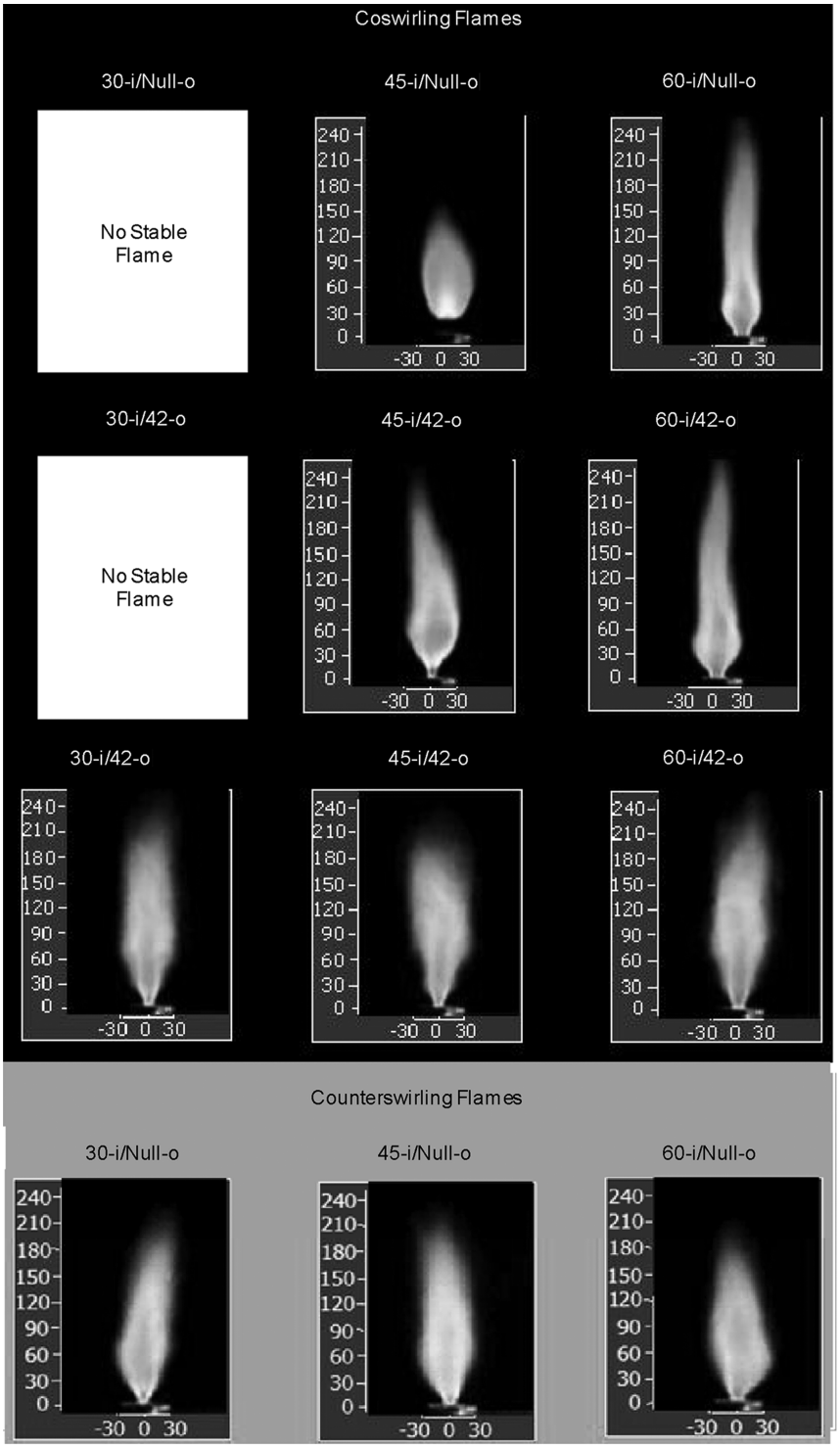

Fig. 7 Effect of swirl configuration on spray flames. Dimensions in the axial and radial directions are in millimeters.

produced the most dramatic effect. In this case, the separation between the near-field and far-field recirculation regions was complete. Because this case corresponded to the airflow features used in the flames described previously, the lifting effect seen in the 45-i/null-o flame can be explained. The near-field recirculation region cannot stabilize combustion. Instead, combustion is stabilized at the boundary of the far-field recirculation region, which also accounts for the geometry of the flame and the lifted flame structure.

Table 4 Atomization-air cases

Atomization-air case	Airflow condition 1	Airflow condition 2
1	0.0 g/s	0.0 g/s
2	0.04 g/s	0.08 g/s
3	0.07 g/s	0.14 g/s

The examined region of the flow in each flowfield case was somewhat limited. This limitation was addressed by carrying out a series of carefully indexed experiments at increasing vertical elevations above the injector. The observations were carried out in an effort to map the extent and geometry of the far-field recirculation region associated with airflow condition 2 and atom.-air case 3. The contours of axial velocity were mapped and the data were plotted on the same set of coordinates. The resulting contours of mean axial velocity, showing the near-field and far-field recirculation zones in

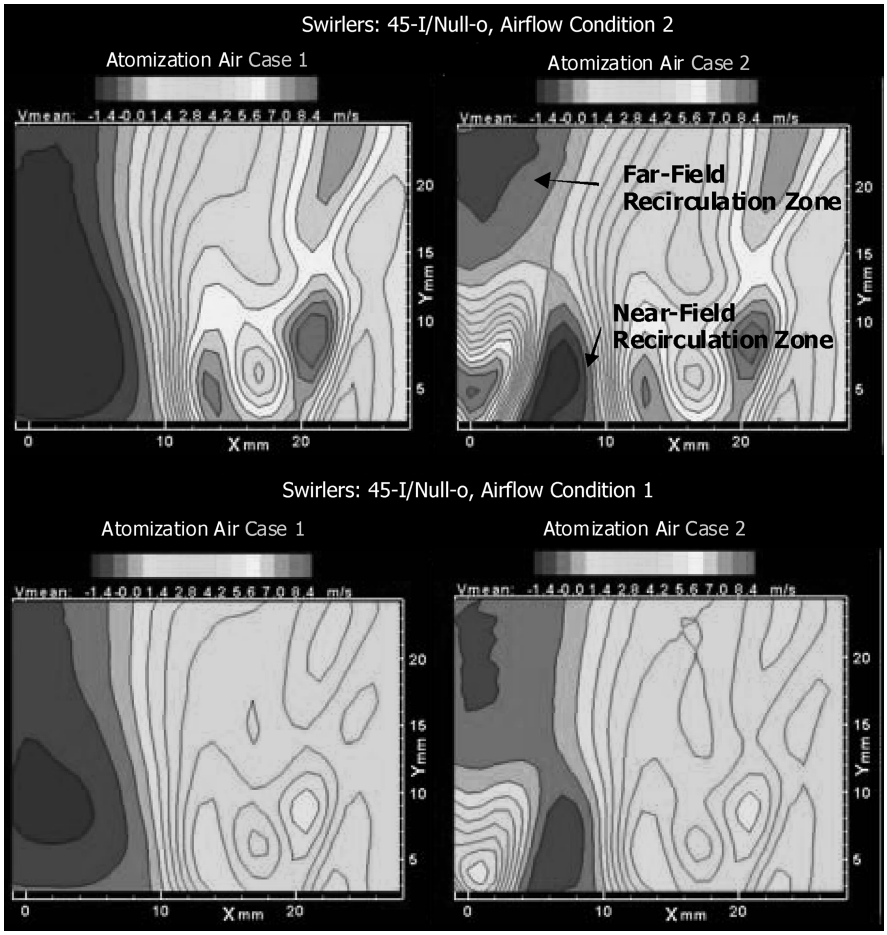

Fig. 8 Mean axial velocity (*V* mean) contours showing effect of atomization-air jet on the airflow field scaled with airflow condition.

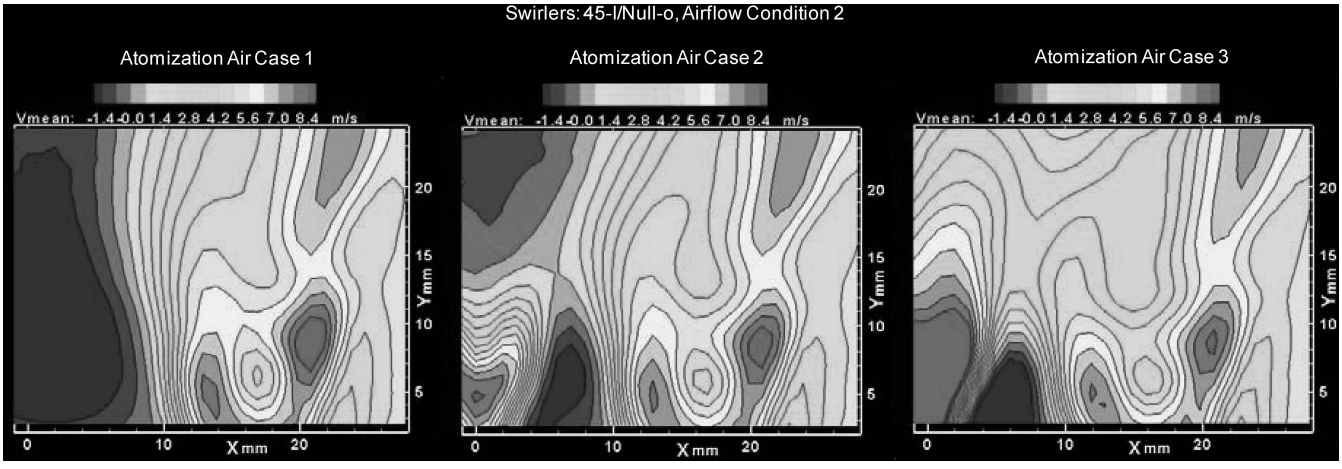

Fig. 9 Mean axial velocity (*V* mean) contours showing effect of atomization-air jet on the airflow field at a single airflow condition.

the 45-i/null-o flow, are shown in Fig. 10. The features of the nonreacting airflow correspond to the 8.2 kW (45-i/null-o swirl) flame shown in Fig. 8. The features of the flow, including the recirculation zones, show a direct connection to the shape of the luminous region of the flame. This correspondence in features is shown more directly in Fig. 11, in which the contour plot and the flame are compared directly on either side of the centerline.

The implications of this observation are significant. It has been known for some time that many features of premixed swirl-stabilized flames depend on the features of the flowfield. However, the results shown in Fig. 11 indicate that the nonreacting-airflow field can also be used to directly analyze the features of much more complex liquid-fueled flames, created using fuel sprays obtained from twin-fluid atomizing nozzles, as examined here.

Thermal effects, droplet evaporation, and other issues associated with the presence of the fuel spray clearly play only a minor role in shaping the flame. The overall volume of the far-field recirculation zone is somewhat larger in the reacting flow, due to heat release, but the shape of the structure is determined by the structure of the airflow. Thus, the momentum fluxes of the swirling airflows and atomization-air jet determine the features of the flow.

D. Effect of Thermal Loading on Flame Geometry

One other factor was found to be important in determining the geometry of the flame. The thermal load of the flame has a significant impact on its length, and the effect of this parameter on the 45-i/null-o flame was examined. Again, an unconfined experiment was

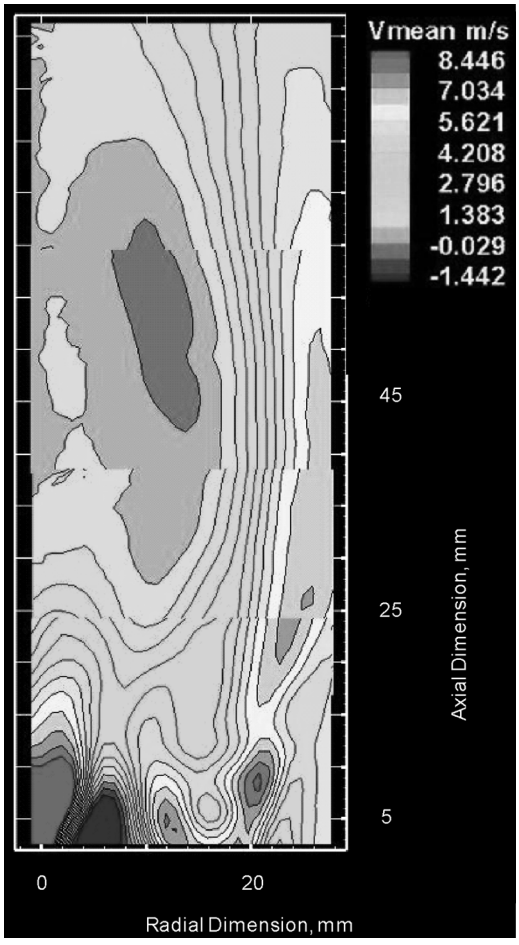

Fig. 10 Mean axial velocity contours showing near-field and far-field recirculation zones.

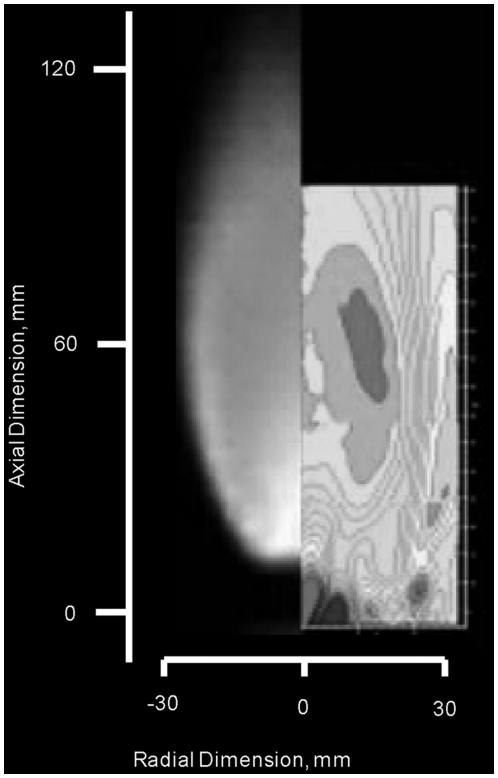

Fig. 11 Comparison of mean axial velocity contours in nonreacting flow and 8.2 kW flame.

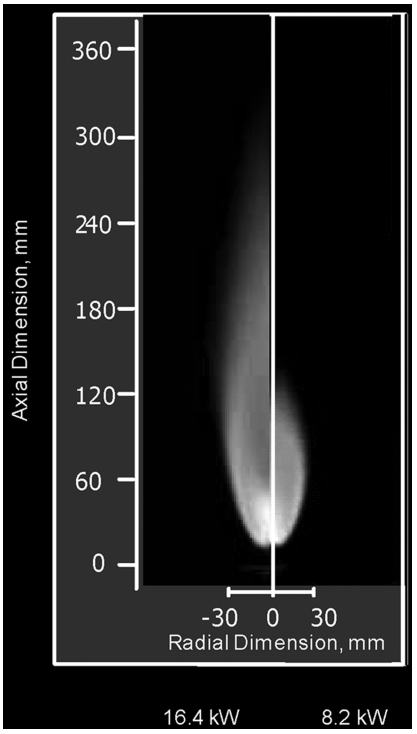

Fig. 12 Comparison of 16.4 and 8.2 kW flames.

undertaken, and airflow rates were set so that airflow condition 2 was obtained. An atomization-airflow rate corresponding to atom.-air case 3 was used to atomize the fuel stream.

The flame was then examined at two different thermal loads. First, the 8.2 kW flame described previously was imaged. Then the fuel flow rate was doubled, so that a thermal load of 16.4 kW was achieved. The flame was imaged again. The two flames are shown in a side-by-side comparison in Fig. 12, with half of each flame on either side of the centerline. The increased thermal load was seen to double the length of the flame.

Other aspects of the flame geometry remained unchanged. The lower edge of the reaction zone remained in the same position at 16.4 kW of thermal loading, as for the 8.2 kW flame. The width of the flame changed only slightly. Essentially, the increased heat release associated with the higher thermal load caused the far-field recirculation region to increase in length, due to the increased expansion of gases in this zone. Features of the flame that were not affected by this downstream heat release, such as the liftoff height, were unaffected by the changes in thermal load. It is not clear on the basis of this set of observations whether the relationship between thermal load and flame length is linear for a wider range of experimental conditions. It appears unlikely that this would be the case, particularly in a confined flame, in which wall interactions would play a role. However, across the range of conditions examined here, the length of the flame does appear to vary linearly with thermal load, at least approximately, and the lifting effect was not impacted by the increase in thermal load.

The effect of thermal load on flame structure also appears to be independent of fuel type. Linck et al. [18] compared the structures of unconfined and confined methanol and kerosene spray flames, in which the flow rates of combustion and atomization air, as well as the thermal load, were equivalent. As can be seen in Fig. 13, the structure of the unconfined flames was very similar for both fuels. The color of the flames was different, due to soot and soot precursors in the kerosene flame that were not present in the methanol flame, but the location, shape, and size of the flames were very similar. This is significant because the volumetric flow rate of methanol fuel is double that of kerosene for an equivalent thermal load. Confined flames at atmospheric pressure, fired at the same thermal load, are shown in Fig. 14. Again, the flame structures appear to be quite similar.

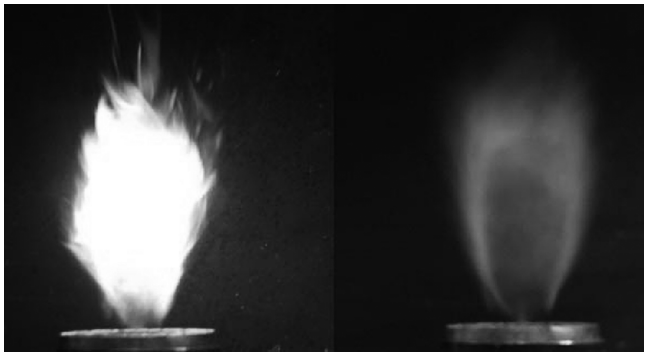

Fig. 13 Unconfined kerosene (left) and methanol (right) flames, at equal thermal load [18].

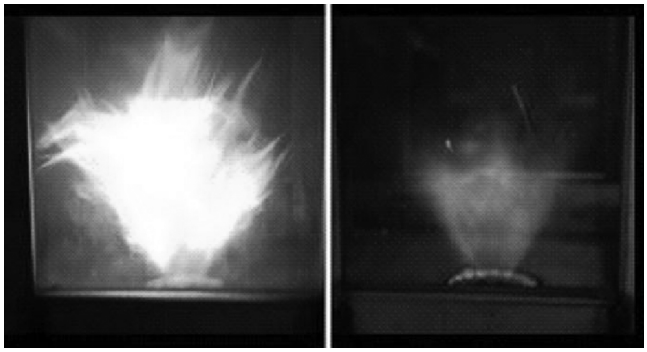

Fig. 14 Confined kerosene (left) and methanol (right) flames, at equal thermal load [18].

The confined kerosene flame looks larger in Fig. 14, but in fact, the flames had very similar structures. In the kerosene flame, luminous particulates allowed the camera to image regions of the flow in which the methanol flame emits very little radiation, and as a result, the image of the kerosene flame appears somewhat larger.

E. Flame Scaling

Thus far, two important factors have been identified that determine, to a great degree, the structure of the reaction zone in the swirl-stabilized spray flame. The results shown here have demonstrated that the flame structure is largely controlled by the airflow parameters and thermal load of the flame. Using this approach, it was possible to create a scaled flame at airflow condition 1 using atom.-air case 3 with an 8.2 kW thermal load that shared many of the features of the 16.4 kW flame (which was created using airflow condition 2 and atom.-air case 3). Note that the atomization-airflow rate was scaled with the Reynolds number of the combustion airflow, so that atom.-air case 3 required that 0.07 g/s of atomization air were fed when airflow condition 1 was applied and required that 0.14 g/s of atomization air were fed when airflow condition 2 was applied. In other words, the flow rates of combustion air through the swirlers, fuel, and atomization air were all reduced by a factor of approximately 2 to create the scaled flame.

Figure 15 indicates that this approach to scaling of flames is valid with certain caveats. The flame shown in the figure was an 8.2 kW flame at airflow condition 1 and did, in fact, closely resemble the 16.4 kW flame at airflow condition 2. There were some differences: for example, the length and shape of the flame were not quite the same. The differences may be due to other factors, such as entrainment of air from the surroundings, the amount of energy needed to vaporize the fuel, relative velocities of droplets in the fuel spray, fuel droplet size distributions, and surface tension effects in the fuel spray. The fuel spray is considered in greater detail subsequently. The flame can at least be approximately scaled if the relationship between airflow and thermal loading parameters is maintained from one operating condition to another. As long as the relationship is the same and the system pressure and effective fuel atomization are maintained, a very similar flame structure should be observed.

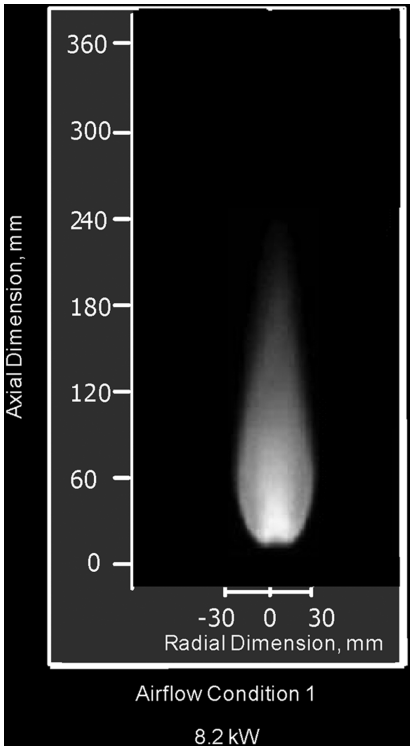

Fig. 15 Scaled 8.2 kW flame.

F. Effect of Airflow Distribution on Flame Structure

Given that the scaled flame at airflow condition 1 and at a thermal load of 8.2 kW seemed to share important structural features with the 16.4 kW flame at airflow condition 2, further experiments were carried out to examine the effect of airflow distribution on the flame structure. The 8.2 kW thermal load was retained, and the total combustion-airflow rate was held constant at 10.94 g/s. Recall that for airflow condition 1, equal volumetric airflow rates were fed through each annulus. The proportion of air fed through the inner and outer annuli was then varied, so that in the first case, only 25% of the total air was fed through the inner annulus and 75% of the total air was fed through the inner annulus. The three distributions examined will be referred to as the 25/75, 50/50, and 75/25 distributions. The swirl configuration was not altered and remained as the 45-i/null-o configuration.

The three flames created by the different airflow distributions are shown in Fig. 16. An increase in the proportion of air fed through the inner annulus increased the overall swirl in the flow, because only the air flowing through the inner swirler had any swirl imparted to it. The flame obtained using the 75/25 combustion-airflow distribution was not lifted; in this case, the swirl in the airflow was large enough for combustion to be stabilized all the way upstream at the fuel nozzle exit. The 25/75 distribution was lifted, and the location at which combustion was initiated occurred at the same axial location as in the flame obtained with the 50/50 distribution. The flame from the 25/75 distribution was narrower and longer than those from the other distributions.

The most compact flame was still the one produced by the 50/50 airflow distribution. Increasing the amount of swirl in the flow (as was the case with the 75/25 distribution) did not necessarily produce a more compact flame. The factors controlling the flame geometry are more complex; mixing, droplet evaporation, and heat-release location all play a role in shaping the reaction zone, and these factors are linked to the flowfield characteristics in complex ways. These phenomena represent an avenue of further examination.

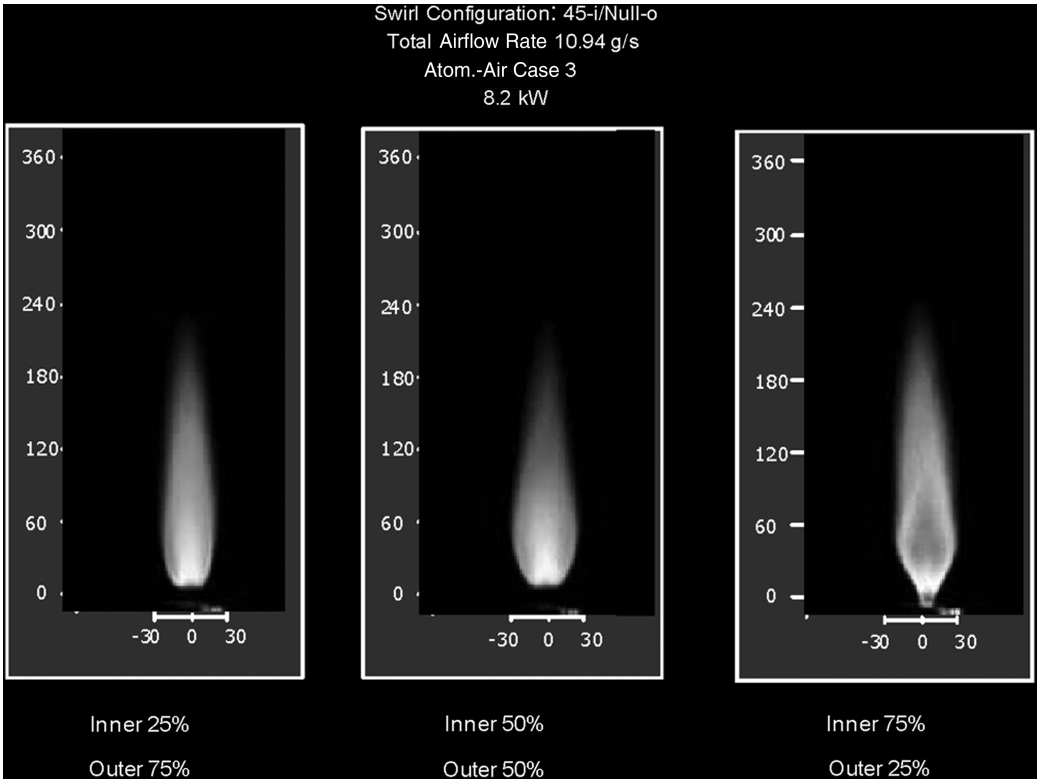

Fig. 16 Effect of airflow distribution on scaled 8.2 kW flame.

G. Fuel Spray Characterization

1. Planar Laser Scattering

The structure of the flame has been shown to depend primarily on the flowfield characteristics and on the thermal load. A detailed understanding of the spray characteristics is necessary to develop a thorough understanding of the factors that affect the flame structure.

The 45-i/null-o flame has already been characterized at two scaling conditions. Further aspects of this flame are now considered. Because the flame structure appeared to be optimal when the 50/50 airflow distribution was employed, this condition was also applied during characterization of the fuel spray. The fuel spray was examined under airflow condition 2 and atom.-air case 3. Thus, 9.3 g/s of air were fed through each of the combustion-air annuli, and 0.14 g/s of atomization air was fed through the fuel nozzle.

Two fuel flow rates were examined. The fuel flow rate of 31 ml/ min corresponded to a thermal load of 8.2 kW. A 16.4 kW thermal load was also examined with a fuel flow rate of 62 ml/ min. The fuel sprays were first imaged under noncombusting and combusting conditions using planar laser scattering. Components of the PIV system, including the lasers and one of the cameras, were used to obtain these images. As in the PIV procedure described previously, a narrow-band-pass filter fitted to the camera optics and a mechanical shutter were used to remove the image of the flame in the combusting cases, thus allowing only images of the droplets illuminated by the laser sheet to be detected by the camera.

Planar laser scattering images of the 8.2 kW fuel spray under noncombusting and combusting conditions are shown in Fig. 17. Images of the 16.4 kW fuel spray under noncombusting and combusting conditions are shown in Fig. 18. The images are monochrome and have been inverted, so that fuel droplets appear as dark regions in the image. At both fuel flow rates, the fuel formed a solid-cone spray with an included angle of approximately 60 deg. The spray associated with the 16.4 kW fuel flow rate was much denser, particularly near the fuel nozzle. This was reasonable, because the volumetric flow rate of fuel through the nozzle in this case was doubled. The sprays were very symmetrical at both thermal loads.

In the combusting cases, the smaller droplets in the spray were not seen in regions more than 35 mm above the fuel nozzle. This was

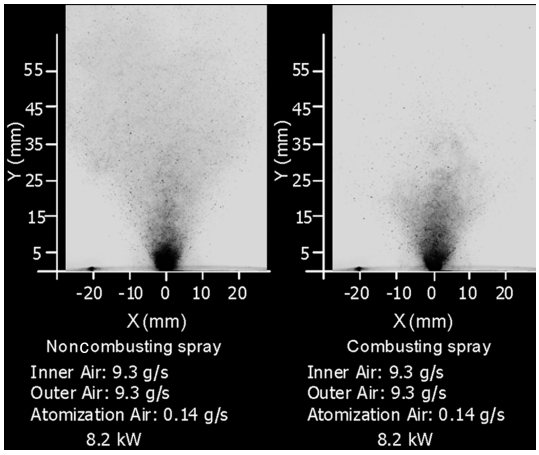

Fig. 17 Fuel spray images, 8.2 kW fuel flow rate.

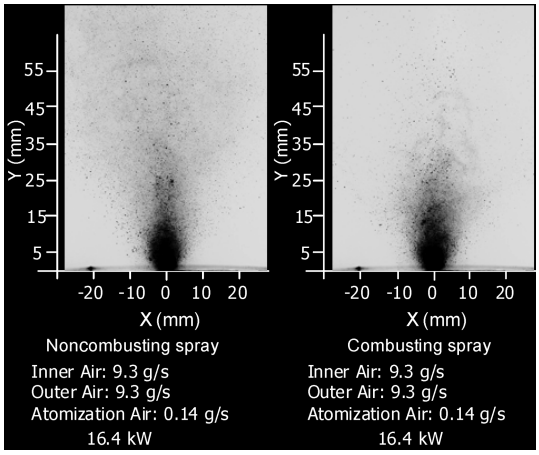

Fig. 18 Fuel spray images, 16.4 kW fuel flow rate.

reasonable, because the heat from the flame eliminated these droplets rapidly. Large droplets also became scarce at elevations over 55 mm above the fuel nozzle. Some isolated droplets with unusually large diameters persisted even further downstream in the flow; this can be seen more clearly in the 16.4 kW spray case.

2. *Phase-Doppler Particle Analysis of Fuel Spray*

More detailed information about the characteristics of the fuel spray was obtained using the PDPA system. Data were gathered on one side of the combustor centerline at an elevation of 35 mm above the fuel nozzle exit. This location was chosen because droplets at this elevation in the spray were fully formed, spaced out widely enough to pass individually through the measurement junction, and only beginning to burn away. Data were gathered at 2 mm intervals until the edge of the spray was reached.

Plots of droplet mean axial velocity and mean radial velocity are shown in Fig. 19. It is apparent that the primary factor influencing the shape of the curves, particularly near the combustor centerline, was the presence or absence of combustion. The 8.2 kW curve and the 16.4 kW curve share the same shape and nearly the same values at every radial location. It should be noted that the number density and consequent volume flux of fuel droplets was lower in the 8.2 kW case than in the 16.4 kW case, due to the smaller amount of fuel present. However, the axial and radial velocities were not apparently influenced significantly by the changes in thermal load, because the atomization-airflow rate was scaled to keep the spray characteristics consistent.

Plots of the arithmetic mean diameter and Sauter mean diameter, referred to as $D10$ and $D32$ in the literature [19], are shown in Fig. 20. Again, the shapes of the curves appear to be influenced more by the presence or absence of combustion than by the fuel flow rate. This is a clear indication that the twin-fluid atomization system employed in the burner provided effective fuel atomization across a wide range of fuel flow rates. The $D32$ was generally larger than the $D10$, as expected, because of the range of droplet sizes observed in the population. The $D32$ is sensitive to large droplets in the spray. Even if they do not occur frequently, they may affect the $D32$ of the entire population. This accounts for the noise seen in the $D32$ curves. Only a few large droplets are necessary to introduce considerable variation into the calculated value of $D32$ at a given location. Again, the spray characteristics were very similar at both thermal loads, whereas the total fuel volume flux was scaled with the thermal load.

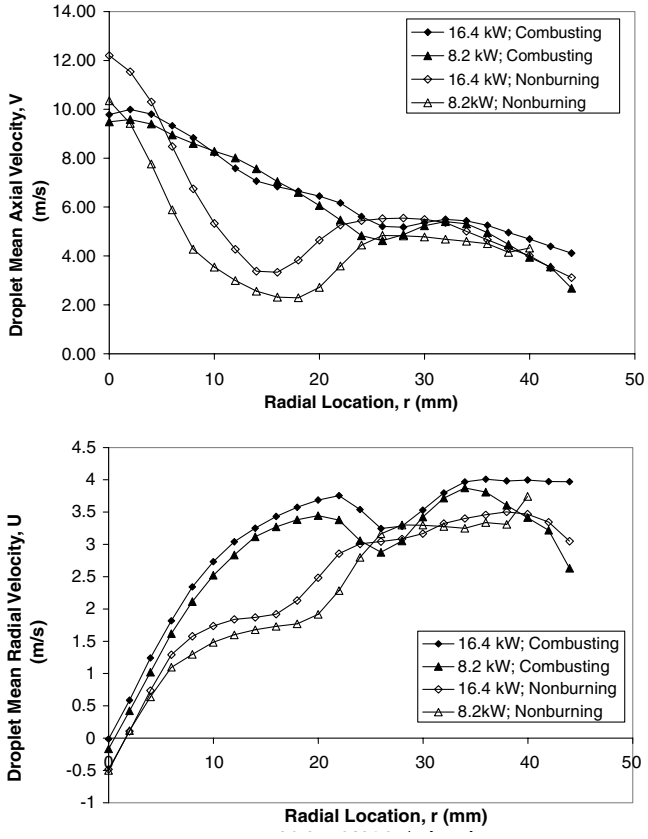

Fig. 19 Plots of fuel droplet mean axial (top) and radial (bottom) velocity.

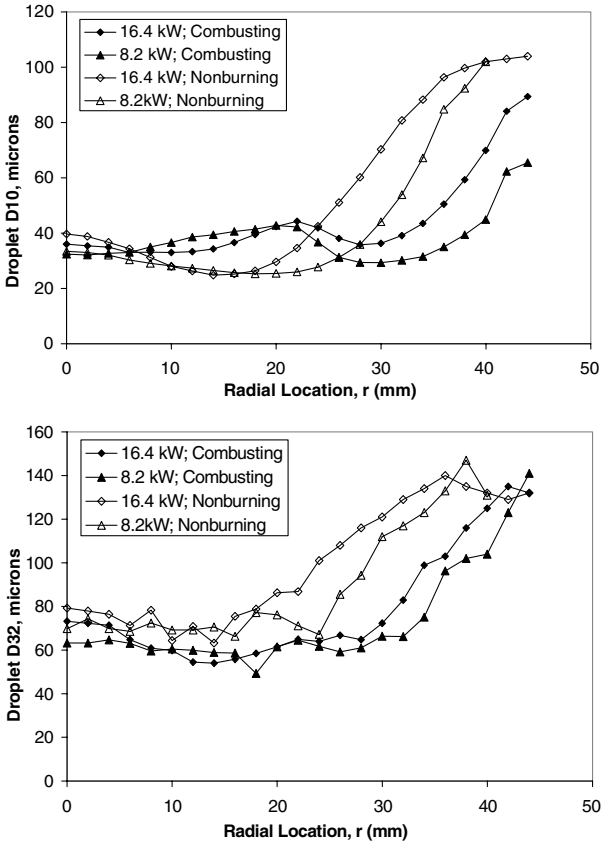

Fig. 20 Plots of droplet mean arithmetic diameter ($D10$, top) and Sauter mean diameter ($D32$, bottom).

3. *Effect of Atomization-Airflow Rate on Fuel Spray*

The effect of the atomization-airflow rate on the fuel spray properties is also important. For both fuel flow rates, the $D10$ and $D32$ were measured at the spray centerline, and the atomization-airflow rate was varied across a wide range. The data gathered are shown in Fig. 21. A certain minimum amount of atomization air is necessary to atomize a given fuel flow rate. Above this minimum, however, the atomization-airflow rate can be varied across a wide

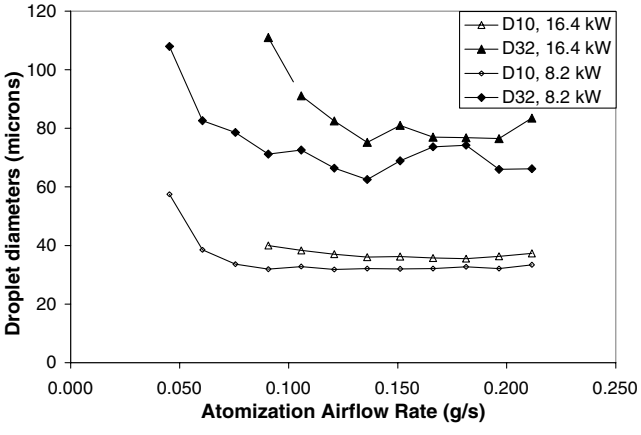

Fig. 21 Effect of increased airflow rate on atomization.

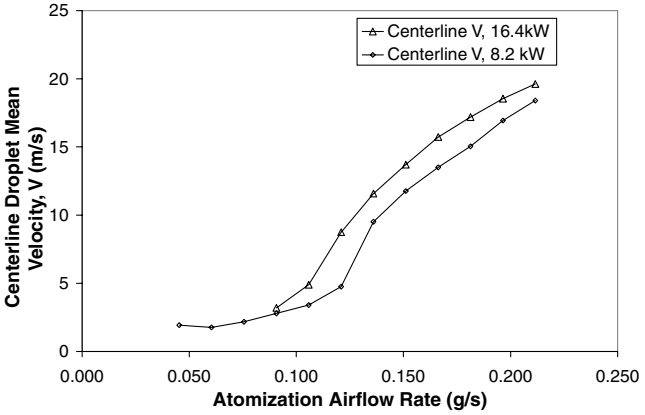

Fig. 22 Effect of increased airflow rate droplet velocity.

range (in this case, from about 0.09 to about 0.21 g/s) without any significant change in the mean droplet diameters. The twin-fluid atomization provides flexible, stable atomization across a wide range of operating conditions, which reveals that atomization-airflow rate and fuel flow rate are not necessarily linked. A given atomization-airflow rate can be set to achieve the correct flame structure, and as long as it is sufficient to provide effective atomization, the fuel will be effectively atomized across a range of power settings.

One characteristic of the fuel spray was found to vary with atomization-airflow rate. The mean velocities of droplets in the spray at the centerline were observed to increase nonlinearly with atomization-airflow rate, as shown in Fig. 22. This effect is not particularly important, however, because it is simply linked to the increasing atomization-air jet velocity. The momentum of individual droplets, 30–50 μm in size, does not appear to have a significant effect on the flame structure. The atomization-air jet plays a much larger role in determining the structure of a flame due to its interaction with the other airflows fed into the burner.

VI. Conclusions

Several points must be made regarding the observations presented in this study. The effect of the atomization-air jet on the structure of the flames investigated is quite significant. The lifting behavior of the flame depends on the relationship between the momentum flux of the atomization-air jet and the swirl strength of the flow. When the flow rate of the atomization air is great enough, relative to the flow rate of the swirling combustion air, two distinct recirculation regions are created. Combustion is stabilized on the outer boundary of the larger far-field recirculation region. If the total swirl imparted to the flow is increased beyond a certain point, the lifting effect is no longer observed. This may imply the existence of some critical relationship between the atomization-air jet and swirl strength. Other parameters, such as the relative swirl strength of the inner and outer combustion airflows, were found to have a less dramatic effect on the geometry of the flame. An inner swirler featuring an outer vane angle of at least 45 deg was necessary to obtain stable combustion in all of the cases examined. An inner swirler with an outer vane angle of 30 deg allowed a flame to be stabilized only if used in combination with outer swirlers featuring outer vane angles of 70 deg. Flames obtained with counter-rotating swirler arrangements were found to be slightly smaller than similar corotating flames, likely due to greater mixing between the counter-rotating flows. However, the lifted flame was significantly more compact than similar nonlifted flames, indicating that this effect may also make it possible to design more compact combustors. The compactness of the lifted flame appears to be due to improved mixing, because the fuel spray is allowed to proceed some distance downstream before interacting with the recirculation zone and flame front. The lifting effect associated with the 45-i/null-o swirl configuration offers the potential to improve combustion control of swirl-stabilized, liquid-fueled systems.

The twin-fluid atomization technique atomized fuel effectively across a wide range of flow rates, even when the atomization-airflow rate was held constant. This demonstrates that the atomization-airflow rate can be adjusted to obtain a particular flame geometry and that the thermal load of the flame can then be controlled by changes in the fuel flow rate.

Other investigators, working with premixed systems, have described lifted premixed flames produced by a unique type of low-swirl injector (LSI). Cheng et al. [20] found that if rotation is imparted to the outer layers of a round, turbulent, premixed jet, the jet expands downstream of the injector and a flame is stabilized in that region of the jet in which the flame speed matches the velocity of the flow. The flames described by Cheng et al. are lifted and do not interact directly with the injector. However, the flames described in the present work differ fundamentally from lifted premixed flames obtained from an LSI. A flame produced by an LSI does not recirculate, and flames of this type have been described thus far only in premixed systems. On the other hand, the lifted flames discussed in the present work do have recirculation regions. Johnson et al. [21] presented a useful comparison of premixed lifted flames created with a low-swirl injector and premixed attached flames created with a more conventional high-swirl injector. Johnson et al. found that lifted premixed flames produced up to 60% less NOx than comparable attached premixed flames. It is possible that similar benefits may be observed if lifted liquid-fueled flames of the type discussed here are compared with more conventional attached liquid-fueled flames.

Acknowledgments

The authors wish to express their sincere gratitude to the Office of Naval Research (ONR), Program Manager, Gabriel Roy, for financial support of the project. Thanks are due also to Ken Yu for his insights and advice and to Guillaume Bourhis for his assistance in constructing the experimental facility used in the experiments.

References

[1] Gupta, A. K., Lilley, D. G., Syred, N., *Swirl Flows*, Abacus Press, Kent, England, U.K., 1984.

[2] Linck, M., "Spray Flame and Exhaust Jet Characteristics of a Pressurized Swirl Combustor," Ph.D. Dissertation, Mechanical Engineering Dept., Univ. of Maryland, College Park, MD, 2006.

[3] Lefebvre, A. H., *Gas Turbine Combustion*, Taylor and Francis, Philadelphia, 1983.

[4] Chigier, N. A., and Beér, J. M., *Journal of Basic Engineering*, Vol. 86, No. 4, 1964, p. 788.

[5] Cohen, H., Rogers, C. F. C., and Saravanamuttoo, H. I. H., *Gas Turbine Theory*, 4th ed., Longman, Essex, England, U.K., 1996.

[6] Linck, M., and Gupta, A. K., "Control of Forced Combustion Instability in a Swirl-Stabilized Spray Combustor via Swirl and Airflow Distribution," *Journal of Propulsion and Power* (to be published).

[7] Glassman, I., *Combustion*, 3rd ed., Academic Press, New York, 1996.

[8] Nasr, G. G., Yule, A. J., and Bendig, L., *Industrial Sprays and Atomization: Design, Analysis and Applications*, Springer, London, 2002.

[9] Ateshkadi, A., McDonnell, V. G., and Samuelsen, G. S., "Effect of Hardware Geometry on Gas and Drop Behavior in a Radial Mixer Spray," *27th International Symposium on Combustion*, Combustion Inst., Pittsburgh, PA, 1998, pp. 1985–1992.

[10] Raffel, M., Willert, C., and Kompenhans, J., *Particle Image Velocimetry: A Practical Guide*, Springer–Verlag, Berlin, 1998.

[11] Anon., *Model 9306A Six-Jet Atomizer Instruction Manual*, Rev. B, TSI, Inc., Shoreview, MN, 2003.

[12] Bernard, P., and Wallace, J. M., *Turbulent Flow: Analysis, Measurement, and Prediction*, Wiley, Hoboken, NJ, 2002.

[13] Mörtberg, M., "Study of Gas Fuel Jet Burning in Low Oxygen Content and High Temperature Oxidizer," Ph.D. Dissertation, Faculty for Energy and Furnace Technology, Kungliga Tekniska Högskolan, Stockholm, 2005.

[14] Anon., *Real-Time Signal Analyzer, Aerometrics Manual*," Aerometrics, Inc., Sunnyvale, CA, 1995.

[15] Bachalo, W. D., and Houser, M. J., "Phase/Doppler Spray Analyzer for Simultaneous Measurements of Drop Size and Velocity Distributions," *Optical Engineering (Bellingham, Washington)*, Vol. 23, No. 5, Sept. 1984, pp. 583–590.

[16] Presser, C., Gupta, A. K., Avedisian, C. T., and Semerjian, H. G., "Effect of Dodecanol Content on the Combustion of Spray Flames,"

Atomization and Sprays, Vol. 4, No. 3, 1994, pp. 207–222.

[17] Linck, M., and Gupta, A. K., "Effect of Swirl and Combustion on Flow Dynamics in Luminous Kerosene Spray Flames," 41st AIAA Aerospace Sciences Meeting, AIAA Paper 2003-1345, Reno, NV, Jan. 2003.

[18] Linck, M., Yu, K. H., and Gupta, A. K., "Dynamics of Unconfined and Confined Methanol and Kerosene Spray Flames," 2nd International Energy Conversion Engineering Conference (IECEC), AIAA Paper 2004-5503, AIAA Providence, RI, Aug. 2004.

[19] Fleming, J. W., Sheinson, R. S., and Maranghides, A., "Water Mist Monitoring in Large-Scale Suppression Research: Fundamental Issues," *Proceedings of the Halon Options Technical Working Conference*, Center for Global Environmental Technologies, Univ. of New Mexico, Albuquerque, NM, 24–26 Apr. 2001.

[20] Cheng, R. K., Shepherd, I. G., Bedat, B., and Talbot, L., "Premixed Turbulent Flame Structures in Moderate and Intense Isotropic Turbulence," *Combustion Science and Technology*, Vol. 174, No. 10, Oct. 2002, pp. 29–59.
doi:10.1080/713712911

[21] Johnson, M. R., Littlejohn, D., Nazeer, W. A., Smith, K. O., and Cheng, R. K., "A Comparison of the Flowfields and Emissions of High-Swirl Injectors and Low-Swirl Injectors for Lean Premixed Gas Turbines," *Proceedings of the Combustion Institute*, Vol. 30, Jan. 2005, pp. 2867–2874.
doi:10.1016/j.proci.2004.07.040

D. Talley
Associate Editor